Phys. Status Solidi A **206**, No. 8, 1833–1837 (2009) / **DOI** 10.1002/pssa.200881609

physica status solidi a
www.pss-a.com
applications and materials science

Elliptical micropipes in SiC revealed by computer simulating phase contrast images

Tatiana Argunova[1,2], Victor Kohn[3], Ji-Won Jung[2], and Jung-Ho Je[*,2]

[1] Ioffe Physico-Technical Institute, RAS, Polytekhnicheskaya st., 26, 194021 St. Petersburg, Russia
[2] X-ray Imaging Center, Pohang University of Science and Technology, San 31, Hyoja-dong, Namku, 790784 Pohang, Korea
[3] Russian Research Center "Kurchatov Institute", Kurchatov sq., 1, 123182 Moscow, Russia

Received 18 September 2008, revised 27 February 2009, accepted 24 March 2009
Published online 23 June 2009

PACS 41.50.+h, 61.05.cc, 61.72.Dd, 61.72.Lk

* Corresponding author: e-mail jhje@postech.ac.kr, Phone: +82 054 279 8081, Fax: +82 054 279 2992

The elliptical micropipes in SiC are studied using computer simulation of the phase contrast images. The experimental measurements of "white beam" images are performed at third-generation synchrotron radiation source in Pohang, Korea. We reveal that the transmitted X-ray spectrum of a high brilliance with a pronounced maximum at 16 keV enables to form partially coherent images even for transparent objects. The computer simulation allows one to automatically determine the diameters of elliptical cross-sections based on best matches between calculated and experimental intensity profiles. We show that the micropipes studied here have extended elliptical cross-sections, sometimes rotating around the micropipe axis.

1 Introduction Physical properties of SiC are well adapted for power electronic devices. The structural defects of micropipes (MPs) that are formed during the growth of SiC bulk single crystals are, however, very harmful to electrical device performance, causing breakdown point-failures in power devices.

One possible explanation of the origin of MPs, as suggested by Frank [1], is the elimination of high elastic stresses around screw dislocations via the formation of pipes. Indeed, the data obtained with various methods such as optical, scanning force (SFM) and scanning electron (SEM) microscopies [2, 3], conventional X-ray and synchrotron white beam topographies (SWBXT) [2, 4], and transmission electron microscopies (TEM and HREM) [3, 5] show that micro and nanopipes are caused by screw dislocations. However, the dependences of the MP radii on their Burgers vectors observed by different authors demonstrated quantitative discrepancies. To make them consistent with the Frank theory, Heindl et al. [6] suggested a hollow core dislocation as mixed rather than screw.

Comprehensive theoretical analysis of hollow core dislocations [7, 8] has not been experimentally confirmed so far. The anisotropic strain around MPs that was observed using polarized light microscopy (PLM) [9, 10] was attributed to the superposition of elastic strains of MP and the edge dislocation trapped at MP [9]. (Afterwards screw dislocation nature of MPs was confirmed by the correlation of these defects using PLM and SWBXT [11].) Importantly, MPs in crystals interact with one another or other lattice defects [12–15] affecting their morphology. A clear picture of MP morphology in SiC crystals has yet to be studied.

A direct non-destructive method to study MP structure in crystal interior is synchrotron radiation (SR) phase contrast imaging [16]. Third-generation SR sources of small angular size provide an excellent spatial coherence. Monochromatic X-rays are prepared by crystal monochromator that extracts a narrow spectral band (typically $\Delta\lambda/\lambda \cong 10^{-5}$) out of the white beam [17, 18]. Such a high monochromaticity is not required for objects with a relatively small transverse size. Actually imaging can also be realized with a low resolution monochromator [19] or without a monochromator at all, i.e., in a "white beam" [13, 14]. The white beam phase contrast technique has several advantages compared to monochromatic beam, namely, high intensity, high time-resolution, large imaging area and simplified experimental setup [13, 14, 19]. The high intensity allows us to carry out better processing of data with small contrast including subtracting the artifacts. Using phase contrast imaging in a white beam we have studied the location and orientation of MPs [13–15]. Recently we developed computer simulation

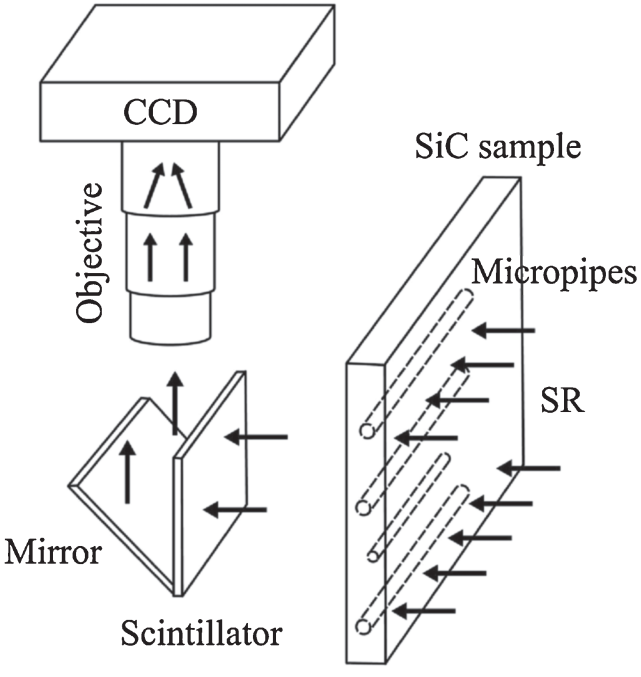

Figure 1 The experimental set-up for white beam phase imaging. Polychromatic SR falls on an SiC sample at 34 m from the source. Image is recorded at various sample–scintillator distances.

of phase contrast images to characterize MP structure quantitatively [20].

In this work, we present computer simulation of the phase contrast images of elliptical MPs to determine the parameters of the elliptical cross-section. Experiments are performed using white beam, at a third-generation SR source (Pohang Light Source, Pohang, Korea). We reveal that the transmitted X-ray spectrum of a high brilliance with a pronounced maximum at 16 keV enables to form partially coherent images even for transparent objects. We show that the MPs studied here have extended elliptical cross-sections, sometimes rotating around the MP axis.

2 Experiment Figure 1 shows the experimental set-up used for phase contrast imaging. The measurements were performed at the 7B2 X-ray Microscopy Beamline with an effective source size of the order of 60 μm (160 μm) in the vertical (horizontal) direction. The source-to-sample distance was 34 m. No optical elements, including monochromator, except beryllium windows and polymer film were used. X-ray image was converted into visible one by 150 μm thick $CdWO_4$ scintillator and magnified by a lens system with magnification from 1× to 50× before recorded with a charge coupled device camera (14-bit gray scale and 1600 × 1200 pixels range). A sample stage with three rotational axes and three translational motions was utilized.

MP images are affected by many factors such as beam parameters and spectrum, the pipe cross-section, the sample-scintillator distance, and the orientation of the pipe axis. The images can be white or black inside with black or white edges;

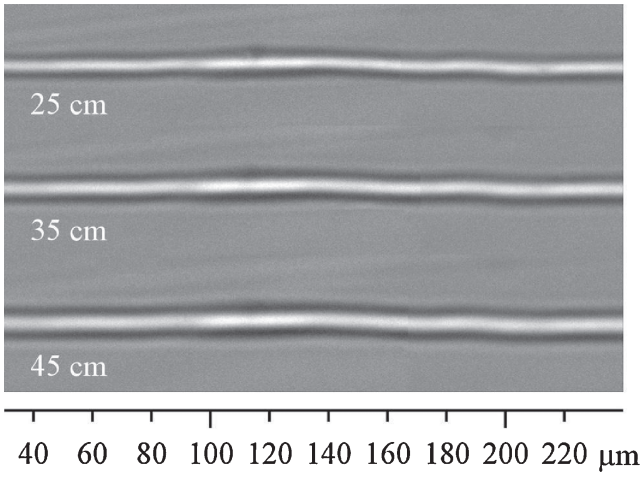

Figure 2 Distance dependence of the MP images. Sample–scintillator distances in centimeters are shown on the image. Distance along the MP is shown below the image.

or else intermediate variants. Interestingly the contrast of MP changes during the rotation of sample, indicating a significant dependence of the contrast on the orientation of MP axis relative to the beam. The aim of computer simulation is to deduce the MP cross-section from fitting simulated intensity profiles to images.

Sample was an axial-cut slice along the growth direction [0 0 0 1] obtained from 4H-SiC boule. The boule was grown by the sublimation sandwich [21] method on $(0\,0\,0\,\bar{1})$ face of 6H-SiC seed in argon atmosphere and in the presence of Sn vapor. The growth temperature was 2180 °C and the growth rate was 0.5 mm h^{-1}. The sample was mechanically polished from both sides down to the thickness of 490 μm. The sample surface was adjusted perpendicular to the beam and rotated to have a horizontal position of the pipe axis, so the MP images were measured in a more coherent vertical direction. We obtained images for nine distances from 5 to 45 cm starting at 5 cm from the sample and increasing the distance every 5 cm.

The distribution of MPs was investigated by combining phase contrast imaging with SWBXT, optical microscopy, and photoluminescence. We observed that the crystal initially grown with a good quality was deteriorated by the appearance of other polytype inclusions, 6H and 15R. A significant amount of MPs (0.5–10 μm in diameter) was generated from the surfaces of these layered polytype inclusions. MPs bundled into groups and interacted. For the purpose of the present study, we have chosen an isolated MP that propagated parallel to the growth axis. Figure 2 shows several typical images of this MP. One can see that the images are sensitive to the distance because of their coherent nature. The intensity profiles were measured at short sections of the whole image.

3 Theory and computer simulation For computer simulation of SR white beam images we have to know the real radiation spectrum which is effectively registered by a CCD. As is known, an initial radiation spectrum is very broad. Each

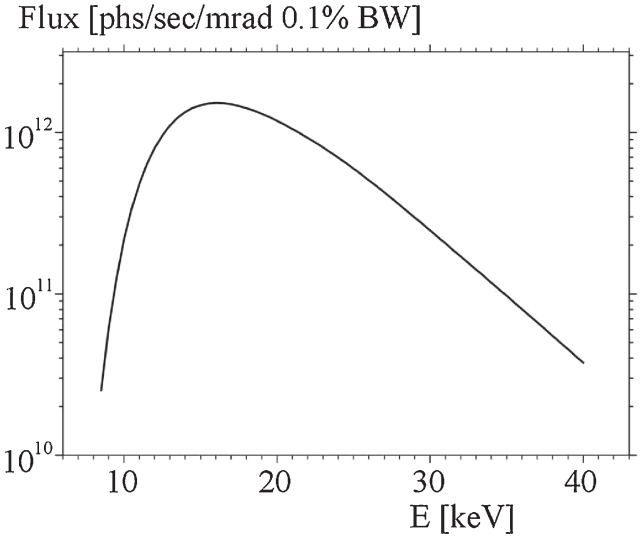

Figure 3 SR spectrum estimated with the absorbers of 2 mm thick Be and 490 μm thick SiC.

photon is excited almost instantly and represents a coherent superposition of harmonics extending from the optical range to the region of few hundreds keV. Since different photons have random phases and an image is summed up over an enormous amount of photons, a real pattern can be calculated on the assumption that various harmonics are incoherent. Besides various harmonics have different intensities which exponentially decrease starting from 5 keV. On the other hand, low energies are absorbed inside all objects in the beam path including the sample itself.

As a result, even in a white SR beam, an image is effectively created in a confined energy range which should be calculated considering all details of experimental set-up including the sample itself. An image in a white beam thus arises via the summation of many patterns formed by each monochromatic harmonic considering the real source size, where the patterns of separate harmonics are taken with different weights. Figure 3 represents SR spectrum used for the calculations. The spectrum was estimated taking into account of the absorption by 490 μm thick SiC wafer placed after 2 mm thick Be window. The spectrum curve shows a pronounced maximum at the energy of 16 keV and rapidly subsides with the energy deviation. Thus, despite an absence of the monochromator, the real spectrum forming the image has some finite energy region of higher brilliance around 16 keV. It is of interest that an image calculated for the monochromatic radiation of 16 keV preserves mainly the same structure as in a white beam. Notice, however, that during white beam experiments, the energy is unchangeable and especially invariable.

Generally, in order to calculate a monochromatic image, MP can be represented as a quasilinear object whose electron density undergoes fast and slow changes across and along its axis, respectively. Choosing a relative intensity profile $I(x)$ at any cross-section, one can neglect the dependence along the axis. Under such approximation the intensity is described as follows:

$$I(x) = |a(x_0)|^2, \quad a(x_0) = \int \mathrm{d}x_1 P_K(x_0 - x_1, Z) T(x_1),$$
$$x_0 = x\frac{z_0}{z_t}, \tag{1}$$

where z_0 is the source–object distance, z_1 is the object-to-detector distance, $z_t = z_0 + z_1$, $Z = z_0 z_1 / z_t$. The problem thus comes to the convolution of two functions.

One function is the Kirchhoff propagator:

$$P_K(x,z) = \frac{1}{(i\lambda z)^{1/2}} \exp\left(\mathrm{i}\pi \frac{x^2}{\lambda z}\right), \tag{2}$$

which corresponds to a reduced distance Z. Here λ is the wavelength of monochromatic radiation. The Kirchhoff propagator describes the propagation of coherent wave in vacuum. The second function $T(x)$ represents the impact of the object on the coherent wave. Since the object size in longitudinal direction is small, it is sufficient to consider the variations of phase and wave amplitude within the limits of geometrical optics, without taking account of ray paths, i.e., presuming that all rays are parallel to z-axis. For a pore with an elliptical cross-section, such approximation allows to exclude a homogeneous sample region, considering the wave distortion caused only by inhomogeneity.

Then, $T(x) = 1$ if $|x| > R$ whereas if $|x| < R$

$$T(x) = \exp\left[(\mathrm{i}P + M)\left(1 - \frac{x^2}{R^2}\right)^{1/2}\right],$$
$$P = \frac{4\pi}{\lambda}\delta R_0, \; M = P\frac{\beta}{\delta}. \tag{3}$$

Here R, R_0 are the radii of the elliptical cross-section perpendicular to the beam (along x) and parallel to the beam (along z). Doubled values, i.e., the diameters of the elliptical cross-section, are in advance unknown; they are required parameters.

Since the integrand in Eq. (1) does not decrease at infinity, for a numerical calculation the integral can be reduced to

$$a(x_0) = 1 + \int \mathrm{d}x_1 P_K(x_0 - x_1, Z)[T(x_1) - 1]. \tag{4}$$

Intensity profiles were calculated for 71 harmonics in the interval between 5 and 40 keV with a constant step of 0.5 keV and summed up taking into account of the spectrum shown in Fig. 3. Computer simulation was done with the FIMTIM program (Fit Micro-Tube Imaging) written in Java and ACL (Advanced Command Language) [22, 23]. The convolution (4) was calculated by means of double Fourier transformation using the algorithm of the fast Fourier transform (details can be found in Ref. [24]). The calculation was done over the net of 4096 points (2048 points for an automatic fit), and the

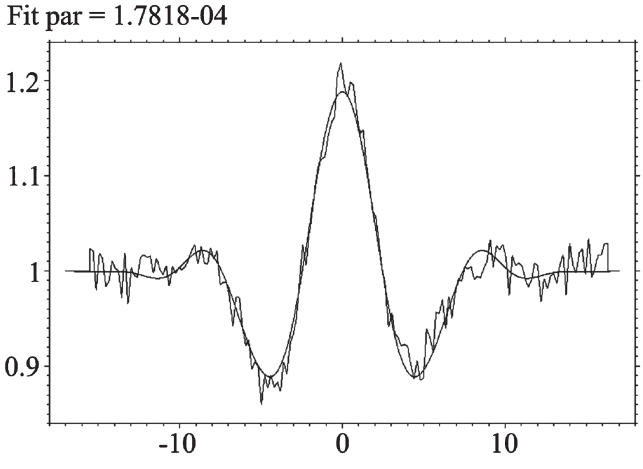

Figure 4 Typical graphs registered by FIMTIM computer program. Sample–scintillator distance is 45 cm. Transverse and longitudinal section sizes are equal to 5.8 and 1.2 μm, respectively. Vertical axis represents intensity in arbitrary units; horizontal axis shows the distance across the MP image in microns.

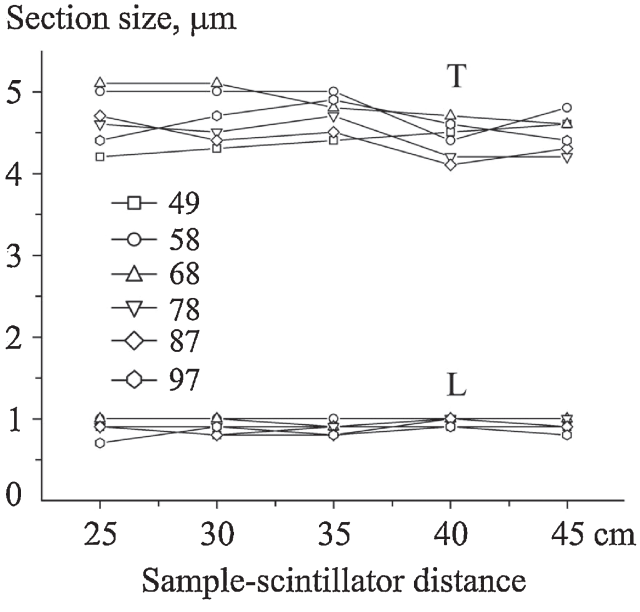

Figure 5 Section size parameters obtained from the images registered at different distances from the sample for six levels along the MP axis. The levels in microns are shown on the graph. T: transverse and L: longitudinal section sizes.

region size was an input parameter (generally 34 μm). The program read a normalized experimental intensity profile; then calculated the profile using formulae (1) and (4) for predetermined R, R_0; interpolated the experimental profile using the points of the calculation net and evaluated the sum of square deviations. At every step the graphs of experimental and calculated profiles were saved. The typical graph is shown in Fig. 4. By sequential adjustment of the parameters R, R_0, we arrived at the best match to the experiment. Notice that it often worked with a very good accuracy. The parameters could be varied by user as well as via automatic procedures. One procedure merely calculated all points over a square net. The other procedure looked for the best fit through the calculation of the points closest to the given point at every step, and arrived at the best matching point. At the same time, earlier calculated points remained unchanged.

4 Results It is known that phase contrast image of a transparent object is not a replica of this object, but is as such a hologram of a special type. At the same time, the image of the same object recorded at different distances, firstly, enlarges and secondly, changes its structure. For this reason, in Ref. [20] we suggested to compare a whole series of images obtained from the same MP at different distances. We assumed that the MP itself had a cylindrical cross-section, and, in fact, evaluated the average radius of this cross-section.

However, a further refined analysis done with the FIMTIM program showed that the assumption of a cylindrical cross-section was not always correct. A studied MP can have an extended elliptical cross-section and, in addition, the cross-section can turn about the MP axis. On the other hand, under such conditions, the measurement of the same cross-section at different distances requires a precise set-up adjustment. Otherwise, the image will infallibly displace with the distance, and different distance measurements should be fitted separately. When evaluated correctly, parameters are independent from the distance. In this approach such independence of the parameters from the distance appears to be a criterion for the correctness of the both experiment and fitting procedure.

Figure 5 shows the section size determined by fitting the data measured at different distances for six close cross-sections located in the interval between 49 and 97 μm along the MP displayed in Fig. 2. One can see that the obtained parameters slightly differ between the distances as well as the cross-sections. Nevertheless, a longitudinal diameter is of the order of 1 μm, while a transverse diameter is about 5 μm. This result is quite unexpected and obtained for the first time. Interestingly, the other part of the same MP exhibits twisting: with distance along the pipe axis its section size changes. Figure 6 represents the section size according to the distance along the pipe; the diameters were obtained by averaging out of the values measured at three sample-scintillator distances: 55, 50, and 45 cm. Even though the accuracy of the evaluation is not high, it allows one to demonstrate that the beam-extended elliptical cross-section of 0.6 μm transverse and 5 μm longitudinal diameters turns quite quickly (over ≈80 μm in length) across the beam.

The results reported here prove that the computer simulation of white beam phase contrast images is an efficient tool to determine the morphology of MPs in SiC crystals. We succeeded to demonstrate that not only the real section size and shape, but also their variation along the MP axis can be

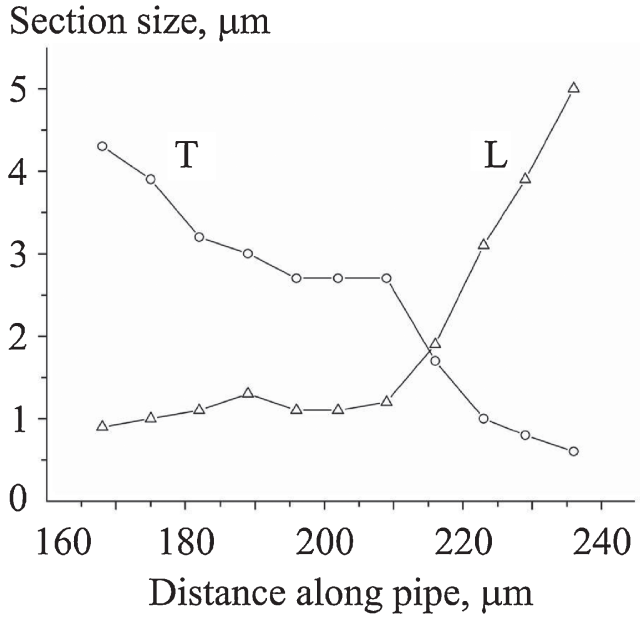

Figure 6 Section size parameters for different distances along the pipe axis determined from the images at three distances from the sample: 45, 50, and 55 cm.

determined. We believe that a further development of this technique will improve the reliability of the results obtained.

Acknowledgements The work of V.G.K. was supported by RFBR Grant Nos. 07-02-00067a and RS-4110.2008.2. The experimental part of this work is supported by the Creative Research Initiatives (Functional X-ray Imaging) of MOST/KOSEF and RFBR under Grant No. 06-02-16244.

References

[1] F. C. Frank, Acta Crystallogr. **4**, 497 (1951).
[2] P. Krishna, S.-S. Jiang, and A. R. Lang, J. Cryst. Growth **71**, 41 (1985).
[3] W. Qian, G. S. Rohrer, M. Skowronski, K. Doverspike, L. B. Rowland, and D. K. Gaskill, Appl. Phys. Lett. **67**, 2284 (1995).
[4] X. R. Huang, M. Dudley, W. M. Vetter, W. Huang, S. Wang, and C. H. Carter, Appl. Phys. Lett. **74**, 353 (1999).
[5] E. Valcheva, T. Paskova, and B. Monemar, J. Cryst. Growth **255**, 19 (2003).
[6] J. Heindl, W. Dorsch, H. P. Strunk, G. St. Müller, R. Eckstein, D. Hofmann, and A. Winnacker, Phys. Rev. Lett. **80**, 740 (1998).
[7] D. J. Srolovitz, N. Sridhar, J. P. Hirth, and J. W. Cahn, Scr. Mater. **39**, 379 (1998).
[8] J. P. Hirth, Acta Mater. **47**, 1 (1999).
[9] H. Ohsato, T. Kato, and T. Okuda, Mater. Sci. Semicond. Process. **4**, 483 (2001).
[10] X. Ma, M. Parker, and T. Sudarshan, Appl. Phys. Lett. **80**, 3298 (2002).
[11] X. Ma, M. Dudley, W. Vetter, and T. Sudarshan, Jpn. J. Appl. Phys. **42** Part 2, L1077 (2003).
[12] W. M. Vetter and M. Dudley, J. Appl. Cryst. **34**, 20 (2001).
[13] M. Yu. Gutkin, A. G. Sheinerman, T. S. Argunova, J. H. Je, H. S. Kang, Y. Hwu, and W.-L. Tsai, J. Appl. Phys. **92**, 889 (2002).
[14] M. Yu. Gutkin, A. G. Sheinerman, T. S. Argunova, J. M. Yi, J. H. Je, S. S. Nagalyuk, E. N. Mokhov, G. Margaritondo, and Y. Hwu, Phys. Rev. B **76**, 064117 (2007).
[15] M. Yu. Gutkin, A. G. Sheinerman, M. A. Smirnov, V. G. Kohn, T. S. Argunova, J. H. Je, and J. W. Jung, Appl. Phys. Lett. **93**, 151905 (2008).
[16] A. Snigirev, I. Snigireva, V. Kohn, S. Kuznetsov, and I. Schelokov, Rev. Sci. Instrum. **66**, 5486 (1999).
[17] P. Cloetens, R. Barrett, J. Baruchel, J.-P. Guigay, and M. Schlenker, J. Phys. D, Appl. Phys. **29**, 133 (1996).
[18] S. Milita, R. Madar, J. Baruchel, M. Anikin, and T. Argunova, Mater. Sci. Eng. B **61/62**, 63 (1999).
[19] Y. Hwu, H. Hsieh, M.-J. Lu, W. L. Tsai, H. M. Lin, W. C. Goh, B. Lai, J. H. Je, C. K. Kim, D. Y. Noh, H. S. Youn, G. Tromba, and G. Margaritondo, J. Appl. Phys. **86**, 4613 (1999).
[20] V. Kohn, T. Argunova, and J.-H. Je, Appl. Phys. Lett. **91**, 171901 (2007).
[21] Yu. A. Vodakov, A. D. Roenkov, M. G. Ramm, E. N. Mokhov, and Yu. N. Makarov, Phys. Status Solidi B **202**, 177 (1997).
[22] See http://java.sun.com for the programming language Java.
[23] See http://vkacl.narod.ru for the programming language ACL.
[24] G. Kohn, I. I. Snigireva, and A. A. Snigirev, Crystallogr. Rep. **51**, S4 (2006).